

A low-cost attempt to improve electrochemical performances of pitch-based hard carbon anodes in lithium-ion batteries by oxidative stabilization

Pin-Yi Zhao^{1,2} · Jia-Ji Tang^{1,2} · Cheng-Yang Wang^{1,2}

Received: 1 August 2016 / Revised: 3 September 2016 / Accepted: 20 September 2016 / Published online: 27 September 2016
© Springer-Verlag Berlin Heidelberg 2016

Abstract The electrochemical performance of low-cost, pitch-based hard carbon anodes in lithium-ion batteries is reported. Pitch-based hard carbon anodes were prepared, stabilized in air at 290 °C for 1 h after different temperature programming, and then carbonized in N₂ at 1000 °C. The optimal anode with temperature programming of 24 h had abundant oxygenic functional groups, a large interlayer space, and a stable morphology. When used as anodes in lithium-ion batteries after 100 cycles at a current density of 100 mA g⁻¹, the capacity was 258.6 mAh g⁻¹ with a capacity retention ratio of 90.6 %. This large capacity combined with the superior cycling performance indicates that prolonged oxidative stabilization is an effective strategy in improving electrochemical performances of lithium-ion batteries.

Keywords Lithium-Ion batteries · Hard carbon · Pitch · Oxidative stabilization

Introduction

The past few decades have witnessed rapid developments of energy storage technologies in fields of portable electronics, electric vehicles, and large-scale rechargeable energy storage due to global demand for green sustainable energy sources

[1–3]. Rechargeable lithium-ion batteries (LIBs) are considered as a potential choice for electric vehicles and have already dominated the portable electronics field [4, 5]. Usually, batteries are composed of a lithium transition metal oxide as a cathode and a carbonaceous anode [6].

The carbonaceous anode, which is primarily determined by the origin of precursor and heat treatment temperatures, strongly influences the capacity of lithium-ion batteries through different intercalation and deintercalation mechanism of lithium ions [7]. Previous research by Dahn et al. [7] categorized carbons into three groups worthy of consideration when it comes to lithium storage: low-temperature carbons, graphitic carbons, and hard carbons. The term “hard carbons” is the description of a kind of highly disordered carbonaceous material originated from some intrinsic non-graphitizable polymeric precursors. It was firstly reported by Takahashi et al. and Sonobe et al. [8, 9]. Recently, the hard carbons have drawn much attention for large-scale LIBs, especially in hybrid electric vehicles because of the superior cyclability and high rate capacities [10]. It has been testified that lithium storage capacity of some hard carbons exceeds that of graphite after heat treatment between 1000 and 1100 °C [11–15]. Thus, electrochemical performances of many different hard carbons have been extensively tested during past decades [16–19], like rice paper [20], sucrose [21], starch [22], phenolic resin [23], and modified pitch [24–26]. However, low carbon yield and high costs of these precursors result in high cost of corresponding hard carbons [27]. Therefore, how to enhance the carbon yield and lower the cost has turned out to be a key step to satisfy requirements for practical applications. As a cheap petrochemical by-product, pitch is widely employed as the carbon source for hard carbons because of the high carbon content and low cost [26, 27]. Thus, great progress would be made if we succeed in fabricating high-performance, low-cost, and pitch-based carbonaceous anodes.

✉ Cheng-Yang Wang
cywang@tju.edu.cn

¹ Key Laboratory for Green Chemical Technology of Ministry of Education, School of Chemical Engineering and Technology, Tianjin University, Tianjin 300072, People's Republic of China

² Collaborative Innovation Center of Chemical Science and Engineering (Tianjin), Tianjin 300072, People's Republic of China

Previous research indicates that an intrinsic paradox of hard carbon materials is the decreasing interlayer distance which would lead to a better coulombic efficiency but declining capacity when heat treatment temperatures increase [7, 28]. In order to come up with some feasible solutions to this issue, the heat treatment process of pitch needs to be discussed. Pitch is usually considered as an easily graphitized carbon precursor [25]. The heat treatment within 400–500 °C brings about aromatic condensation reactions of polycyclic aromatic constituents and ends in highly oriented carbonaceous mesophase which is an intermediate to graphitic carbons. But this natural tendency can be terminated by oxidative stabilization, then less-ordered structures remain. During oxidative stabilization, oxygen as carbonyls is introduced, accompanied by a weight gain and a loss of methylene hydrogens [29]. Therefore, the amount of these oxygen functional groups is supposed to be highly related with the extent of stabilization [30]. Generated oxygen functionalities lead to cross-linking, which forestalls pitch melting and keeps less-ordered carbon structure and larger interlayer space during the following carbonization [31]. Since one intrinsic paradox of hard carbon materials is the trend of a decreasing interlayer distance which is unfavorable for the capacity and a more ordered structure which is favorable for coulombic efficiency when carbonization temperature increases [32], the attempt of oxidative stabilization may lead to a larger capacity by virtue of a larger interlayer distance.

Herein, an isotropic petroleum pitch with a high softening point is selected as the precursor to prepare hard carbons by simple methods of oxidative stabilization and carbonization. The microstructure of pitch-based hard carbons is characterized and corresponding anodic performances are investigated and optimized. Pitch exhibits better electrochemical performances after slower oxidative stabilization, which are attributed to the stable morphology, maintained turbostratic structure, and a larger interlayer space.

Experimental

Chemicals

Black bulk pitch precursor was a petrochemical by-product from a chemical plant in Xinjiang province, China. The softening point of the pitch was 274 °C. Element analysis indicates that primary components are carbon (92.1 %) and a small proportion of hydrogen (4.5 %). The content of sulfur, nitrogen, and oxygen were all very small.

Material preparation

The bulk parent pitch was placed in a vacuum drying oven at 60 °C for 12 h after milling. Then, 1.00 g of parent pitch was oxidatively stabilized at 290 °C for 1 h after 6, 12, or 24 h

temperature programming (air flow 150 mL min⁻¹) with different heating rates, respectively. The parent pitch (PP) after 6, 12, or 24 h temperature programming and oxidatively stabilized at 290 °C for 1 h is labeled as PP-290-6, PP-290-12, and PP-290-24, respectively. Time consumed and corresponding rates in the temperature programming process are shown in Table 1. After being stabilized, the pitches were carbonized under a nitrogen flow (flow rate 150 mL min⁻¹) at 1000 °C for 1 h. After carbonization, the samples were labeled as PP-290-6-C, PP-290-12-C, and PP-290-24-C, respectively. A sample carbonized without oxidation is also prepared under the same temperature programming in N₂ (flow rate 150 mL min⁻¹) to contrast with samples after oxidation, denoted as PP-N-290-24-C.

Material characterization

The element analysis was conducted on a Variomicro-CUBE element analyzer. The oxygen content was determined by subtraction of other elements (C, H, N, and S) from 100 %. Thermogravimetric analysis (TG) was tested from 40 to 900 °C at 10 °C min⁻¹ on a TA-50 instrument under nitrogen atmosphere. IR spectra were performed on a Nicolet Magna-560 spectrometer. Scanning electron microscopy (SEM) was conducted with a Nano 430 spectrometer. A Philips Tecnai G2 F20 spectrometer was utilized for high-resolution transmission electron microscopy (HRTEM) measurements. X-ray diffraction (XRD) was performed at 40 kV and 90 mA with Cu K radiation ($\lambda = 0.154056$ nm) on a Rigaku D/Max 2500 instrument. The interlayer distance d_{002} , the a-axis length (L_a), and the c-axis length (L_c) were obtained using Bragg and Scherrer equations [33]. Raman spectra were obtained from a Raman microscope (Renishaw MKI-2000, Ar ion laser as the excitation source). N₂ adsorption measurements were done on a TriStar 3000, GA instrument at 77 K, and the surface areas of the samples were calculated using the Brunauer-Emmette-Teller (BET) equation.

Electrochemical characterizations

Electrochemical performance was tested on a CR2430 coin cell. Stabilized pitch was homogeneously mixed with carbon black and polyvinylidene difluoride binder (mass ratio 8:1:1) in solvent of N-methyl-2-pyrrolidone to get slurry. Then, this slurry was casted on a piece of Cu foil. After vacuum drying, the foil was cut into electrodes. The loading weights of electrodes were

Table 1 Time and corresponding rates during temperature programming

Samples	t (h)	Rate (°C min ⁻¹)
PP-290-6	6	0.611
PP-290-12	12	0.306
PP-290-24	24	0.153

$\sim 1.4 \text{ mg cm}^{-2}$. Before assembling cells, the electrodes were dried in a vacuum drying oven at $120 \text{ }^\circ\text{C}$ for 12 h.

The LIBs were assembled with a lithium plate as the counter electrode, and 1.0 M LiPF_6 was used as the electrolyte in ethylene carbonate and dimethyl carbonate (volume ratio: 1:1).

Galvanostatic charge/discharge performances were tested from 37.2 to 3720 mA g^{-1} between 0 and 2.7 V on a Land Battery Test System. Cyclic voltammetry measurement was made at a scan rate of 0.1 mV s^{-1} between 0 and 2.7 V on an electrochemical workstation (Chenhua Company, China). In this contribution, lithium intercalation into carbon anode is referred as discharge whereas lithium deintercalation is corresponded to charge process. Besides, specific capacities were calculated according to weight of stabilized pitch in electrodes.

Results and discussion

PP was firstly analyzed by TG. TG curves of PP (Fig. 1) show that initial weight loss temperature of the PP is $260 \text{ }^\circ\text{C}$, and after $570 \text{ }^\circ\text{C}$ there is no obvious weight loss. Moreover, the peak at around $470 \text{ }^\circ\text{C}$ in the differential TG curve indicates that PP is losing weight most rapidly at around $470 \text{ }^\circ\text{C}$. Over the temperature range of $30\text{--}850 \text{ }^\circ\text{C}$, the PP loses 53% of its original mass as pitch is usually considered as a mixture of aromatic compounds and volatile small molecules that can be easily decomposed with departure of hydrocarbon skeletons as well as compounds like CO , CO_2 , and CH_4 [34]. Since the stabilization process is very slow and pitch has cross-linked inside during this process, worries that stabilization temperature is higher than softening point of pitch and pitch would become over-soft during the oxidative stabilization are not necessary.

Table 2 is the elemental analysis result of the parent pitch and pitches after various treatments. It is shown that during oxidative stabilization, longer treatment time lead to a gradual

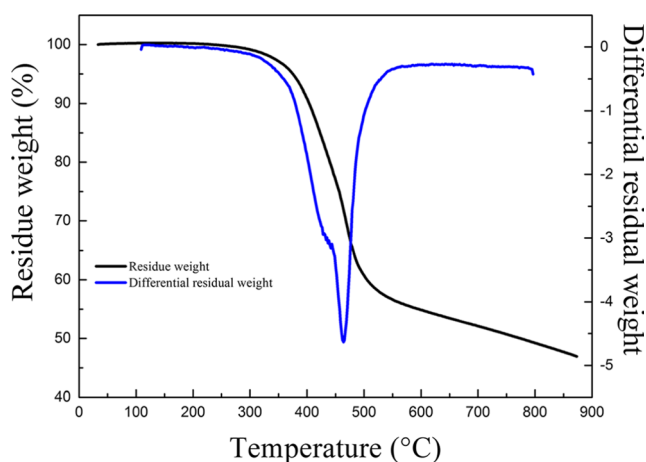


Fig. 1 Weight loss of parent pitch under N_2 atmosphere

Table 2 Elemental analysis of the parent pitch and pitches after various treatments

Sample	Element analysis (wt%)				
	C	H	N	S	O ^a
PP	92.0	4.5	1.0	0.6	1.9
PP-290-6	91.5	4.3	1.1	0.5	2.6
PP-290-12	91.2	4.0	1.1	0.3	3.4
PP-290-24	91.0	3.9	1.1	0.2	3.8
PP-290-6-C	97.9	0.7	0.3	0.3	0.8
PP-290-12-C	97.7	0.6	0.3	0.2	1.2
PP-290-24-C	97.6	0.5	0.3	0.2	1.4

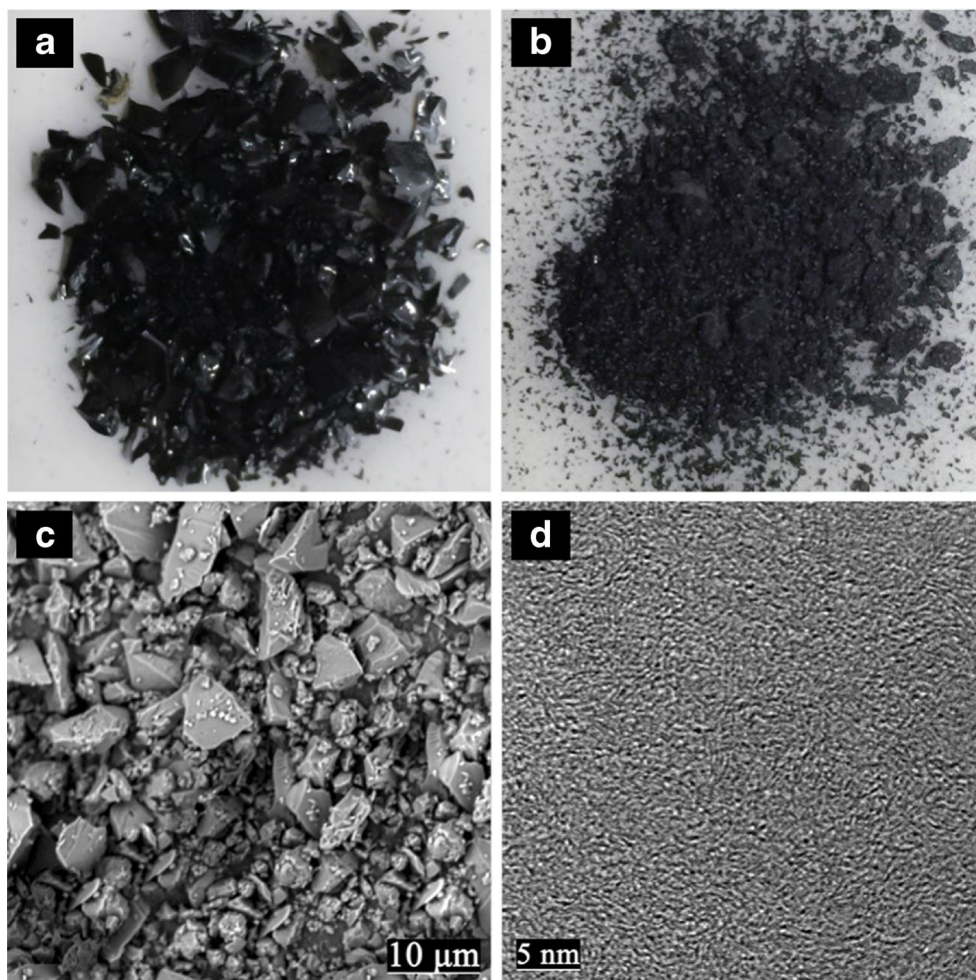
^aOxygen tested by difference

decrease of hydrogen and sulfur contents, whereas nitrogen content was not significantly affected by extended oxidative stabilization. For oxygen content, an increase was observed, which may attribute to an increasing amount of oxygenic functionalities. In addition, the C/H ratio of samples after oxidative stabilization was higher than PP. These results together manifest that pitch underwent dehydrogenation polymerization during stabilization with drastic aliphatic hydrogen loss [31, 35]. After carbonization, differences in values become weaker but trends of values still remain.

Figure 2a, b shows the morphological difference of carbonized samples with or without oxidative stabilization. PP-N-290-24-C appears in bulks as a result of remelting whereas PP-290-24-C keeps the powder macro-morphology, which prove that oxidative stabilization can prevent remelting and maintain a stable morphology after carbonization [10]. SEM and HRTEM of PP-290-24-C are further investigated in Fig. 2c, d, respectively. In Fig. 2c, PP-290-24-C shows a randomly distributed particle size (about $5 \mu\text{m}$) and stable micro-morphology with no remelting. Figure 2d reveals the amorphous nature of PP-290-24-C. After carbonization, PP-290-24-C is still poorly crystallized as a result of hard carbon nature and the parallel short-range stacking of curved and small graphene layers generate disordered porosity, which can be interpreted by the falling cards model [36].

Figure 3a is the IR spectra from 400 to 3250 wave numbers of PP and PP-290-6. PP exhibits two bands of similar intensity at around 1596 and 1442 cm^{-1} . These bands are related with an aromatic carbon ring breathing mode, and the methylene hydrogen “scissoring” mode, respectively [37]. The strong intensity at 1442 cm^{-1} of the methylene hydrogen bending is due to the existence of large quantities of saturated rings in the parent pitch [38]. Notice in Fig. 3a that as a result of methylene hydrogen bending, the peak at 1442 cm^{-1} disappears in the IR spectrum of oxidized pitch, while the carbon stretching mode at 1596 cm^{-1} remains a similar strength. This phenomenon indicates that aliphatic material is consumed quantitatively during

Fig. 2 **a** Photograph of PP-N-290-24-C, **b** photograph of PP-290-24-C, **c** SEM image of PP-290-24-C, and **d** HRTEM of PP-290-24-C



the oxidative stabilization [29]. Another difference in the two spectra is the appearance of a carbonyl stretching band centered at 1704 cm^{-1} in the spectrum of oxidized pitch. Upon close comparison, it appears that the carbonyl band is composed of two bands, one at about 1772 cm^{-1} , and the other at 1734 cm^{-1} . These bands are ascribed to anhydride and ester functionality,

respectively [38], thus indicating existence of oxygenic functionalities. PP displays three peaks in the fingerprint region of the spectrum, which are ascribed to the aromatic out-of-plane hydrogen bending mode. The noticeable attenuation of this triplet after oxidation indicates decay of aromatic hydrogen in the pitch.

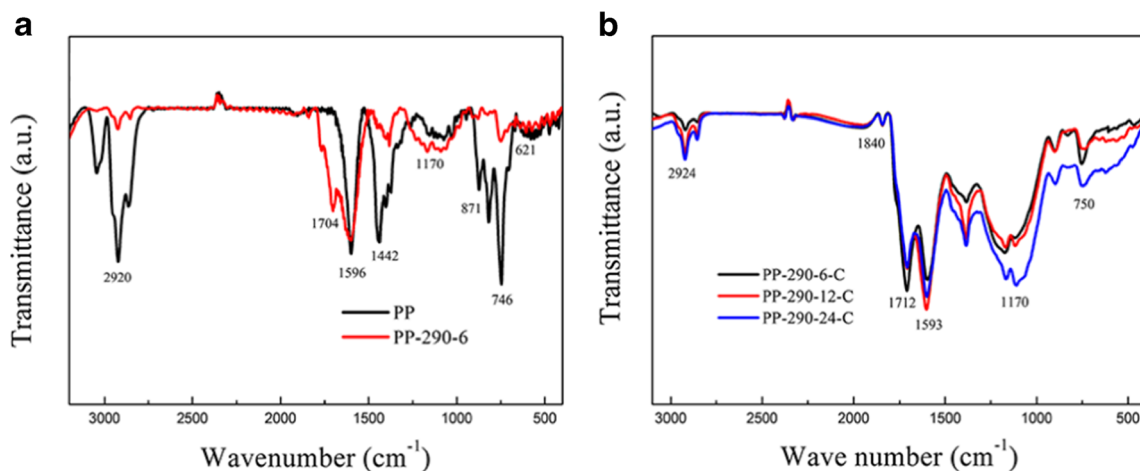


Fig. 3 FT-IR spectra of **a** PP and PP-290-6 before carbonization. **b** Samples after carbonization

Figure 3b displays the IR spectrum of hard carbons treated under different oxidative stabilization conditions. With different temperature programming during oxidative stabilization, intensities of functionalities show miscellaneous behaviors. The peak at around 2924 and 2850 cm^{-1} are related with hydrogen asymmetric or symmetric stretching, respectively. Aromatic carbon-carbon stretching is indicated by peaks at 1593 cm^{-1} . Ketone carbonyls at 1712 and 1840 cm^{-1} undergo slight changes. Peak intensity of ether bonds at 1170 cm^{-1} increases. Peaks of anhydride functionalities are not obvious because during carbonization these functionalities decompose and leave as CO or CO₂ [39].

As is presented in Fig. 4, the galvanostatic charge/discharge curves are measured at a current density of 100 mA g^{-1} . The charge/discharge data are shown in Table 3. Generally, the charge/discharge curves show a precipitous slope, relating to lithium-ion intercalation among graphene layers, whereas a blurry plateau, corresponding to insertion into nanopores [11, 40], is a classical hard carbon behavior [11, 41–43]. The curves are similar with the results from lithium-ion insertion between graphene sheets or binding with hydrogen-terminated graphene sheets [40, 42, 43]. As a result of formation of a solid electrolyte interface (SEI) layer from decomposition of electrolyte and some irreversible insertion of Na into the carbon structure, a common issue of hard carbon materials is the inferior initial coulombic efficiency. Meanwhile, SEI layers can slow the dispersion or decomposition of anodes caused by repeatedly insertion/extraction of sodium ions [44]. Generally, there are two methods to reduce the irreversible capacity [44]. One is suitably raising the carbonization temperature so that there will be fewer irreversible sites, the other is using additive in the electrolyte to promote forming stable SEI

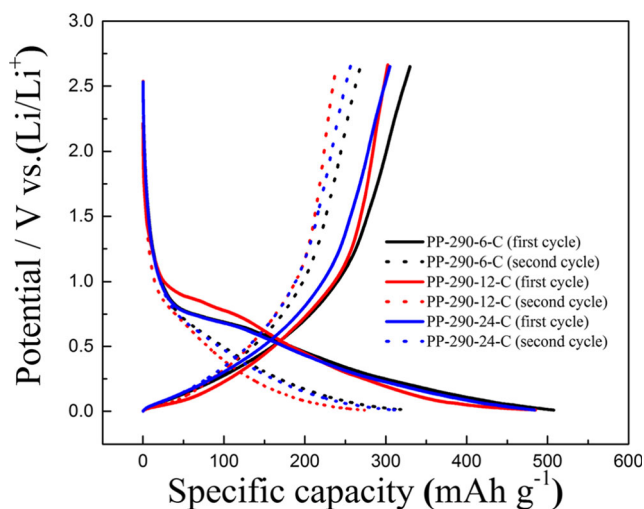


Fig. 4 Galvanostatic charge/discharge profiles for the first two cycles at a current density of 100 mA g^{-1} of PP-290-6-C, PP-290-12-C, and PP-290-24-C

Table 3 Electrochemical properties of the samples

Sample	Q _C ^a (mAh g ⁻¹)	Q _D ^b (mAh g ⁻¹)	CE ^c (%)
PP-290-6-C	329.9	505.9	65.2
PP-290-12-C	305.2	482.9	63.2
PP-290-24-C	308.5	496.7	62.1

^a The first cycle charge capacity

^b The first cycle discharge capacity

^c The initial coulombic efficiency

layers so that less fresh layers will form, which is a reason of low coulombic efficiency [45].

Figure 5a displays the 100-cycle performance of the pitch-based electrodes at 100 mA g^{-1} . Three electrodes exhibit similar minor capacity fluctuation, and among them PP-290-24-C has slightly better performance than PP-290-12-C or PP-290-6-C. The charge capacity of PP-290-24-C after the 100th cycle is 258.6 mAh g^{-1} , which indicates a 90.6 % capacity retention.

Figure 5b displays the rate performance of pitch-based anodes at current densities from 37.2 to 3720 mA g^{-1} . Charge and discharge capacities go down at higher rates. On the other hand, pitch-based electrodes show nice reversibility during cycling. For PP-290-24-C, the coulombic efficiency of the first cycle is only about 55 %, but it quickly enhances to a value (>98 %) at a high current of 372 mA g^{-1} . Charge capacity of PP-290-24-C is 276.9 mAh g^{-1} at 37.2 mA g^{-1} , and drops to 158.7 mAh g^{-1} at 372 mA g^{-1} . Notably, PP-290-24-C exhibits superior rate capability than the other two samples at current densities higher than 372 mA g^{-1} .

The above discussion shows that PP-290-24-C has superior electrochemical performance in terms of larger capacity and better rate performance. Therefore, PP-290-24-C is further investigated in detail. Figure 6a is the cycling performance of PP-290-24-C with coulombic efficiency. Within a relatively narrow band, charge and discharge capacities fluctuate during 100 rounds, but after the 20th cycle they could almost keep a coulombic efficiency greater than 98 %. Figure 6b is CV curves of the PP-290-24-C anode. As is illustrated in Fig. 6b, during the cathodic scan, a reduction peak centered at 0.37 V is observed, corresponding to the lithium ions insertion. Combined with cathodic scan at a low potential range, an oxidative peak at 0.25 V during anodic scan corresponding to the deintercalation of lithium ions confirms the promising application of PP-290-24-C anode in lithium ion storage [46]. In the first cycle, the area of the oxidation peak is much smaller than the reduction peak area, suggesting a large irreversible capacity. During subsequent cycles, the peak area of oxidation increases with an enhancing coulombic efficiency. Similar shapes and area of these curves

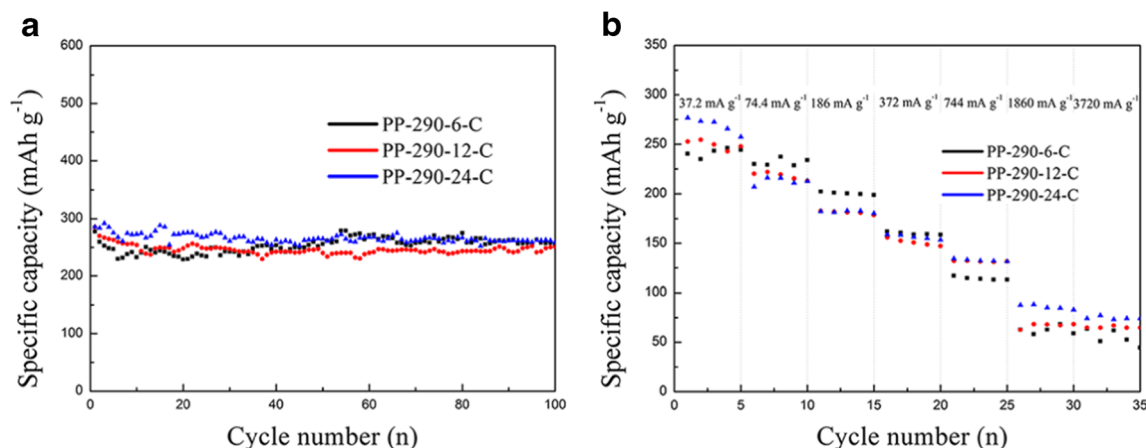


Fig. 5 **a** Cycle performances of electrodes at a constant current density of 100 mA g^{-1} (the batteries were firstly activated 5 cycles at a cycling rate of 20 mA g^{-1}). **b** Rate capabilities of the different pitch-based electrodes at current densities from 37.2 to 3720 mA g^{-1}

suggest that after the first cycle, PP-290-24-C anode delivers stable electrochemical properties.

To illuminate the structure of PP-290-24-C anode and explain its mechanism, Raman spectroscopy is employed to study microstructures of the PP-290-24-C anode. As is displayed in Fig. 7a, the Raman spectrum of PP-290-24-C has a defect-induced mode and a E_{2g} graphitic mode, corresponding to two characteristic bands at $\sim 1350 \text{ cm}^{-1}$ (D-band) and $\sim 1580 \text{ cm}^{-1}$ (G-band) [47]. Compared with PP-N-290-24-C, the intensity ratio (I_D/I_G) of PP-N-290-24-C (0.9707) is smaller than PP-290-24-C (1.0002), indicating a further conversion of disordered carbon to graphitic carbon of PP-N-290-24-C. Thus, it is proved that oxidative stabilization helps maintain turbostratic structure of PP-290-24-C, which may lead to larger capacities of hard carbon anodes.

To further understand the function of oxidative stabilization, an XRD experiment is conducted and compared. Two typical broad amorphous carbon diffraction peaks corresponding to the (002) and (100) diffraction modes at ~ 24 and $\sim 43^\circ$ are shown in Fig. 7b. The broadened peaks indicate tested

materials possess crystallites of tiny sizes [48]. From the XRD analysis, the interlayer space d_{002} of PP-290-24-C is 358 pm , wider than PP-N-290-24-C of $\sim 350 \text{ pm}$. L_c and L_a values of PP-290-24-C are 1.66 and 4.22 nm , respectively. Therefore, lithium ions of the PP-290-24-C anode may gain easier access than the PP-N-290-24-C anode in forming an intercalation compound due to the larger interlayer distance. Besides, the surface areas of the samples were tested and calculated from the Brunauer Emmette Teller equation by a computer software. PP-290-24-C has a surface area around $185 \text{ m}^2 \text{ g}^{-1}$, larger than $133 \text{ m}^2 \text{ g}^{-1}$ of PP-N-290-24-C, which again proves that oxidative stabilization not only prevent remelting, but also helps maintain pore size [10]. Since one important mechanism of lithium storage is that lithium ions intercalate between layers and pores [11, 12, 49, 50], the maintained pore size and interlayer space may contribute to larger capacities and support that oxidative stabilization is an effective method to pursue better electrochemical performances.

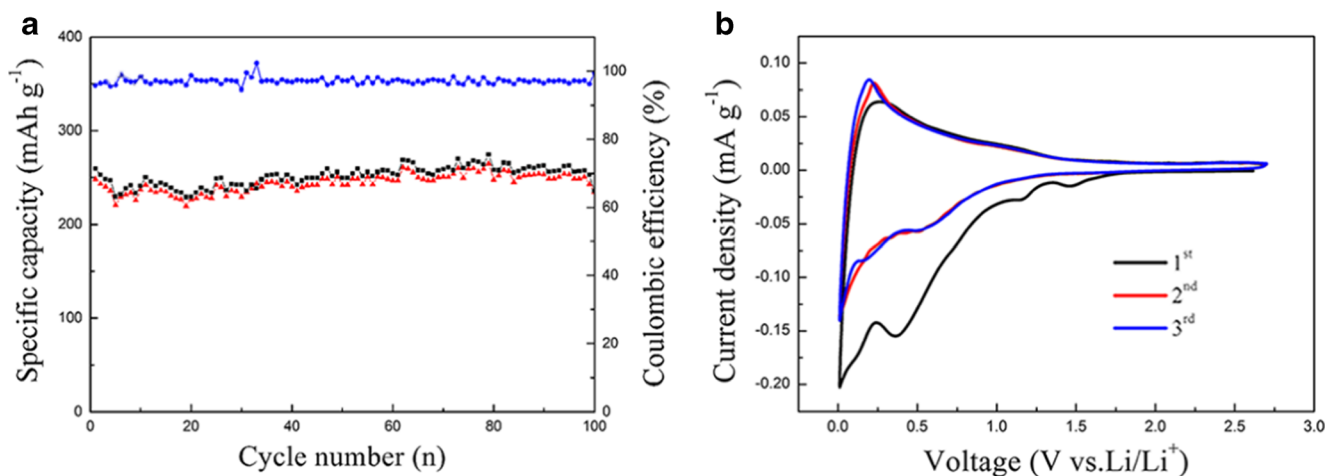


Fig. 6 **a** Cycle performance (the batteries were firstly activated at a cycling rate of 20 mA g^{-1}) and **b** CV curves of the PP-290-24-C anode from 0 to 2.7 V at a scan rate of 0.1 mV s^{-1}

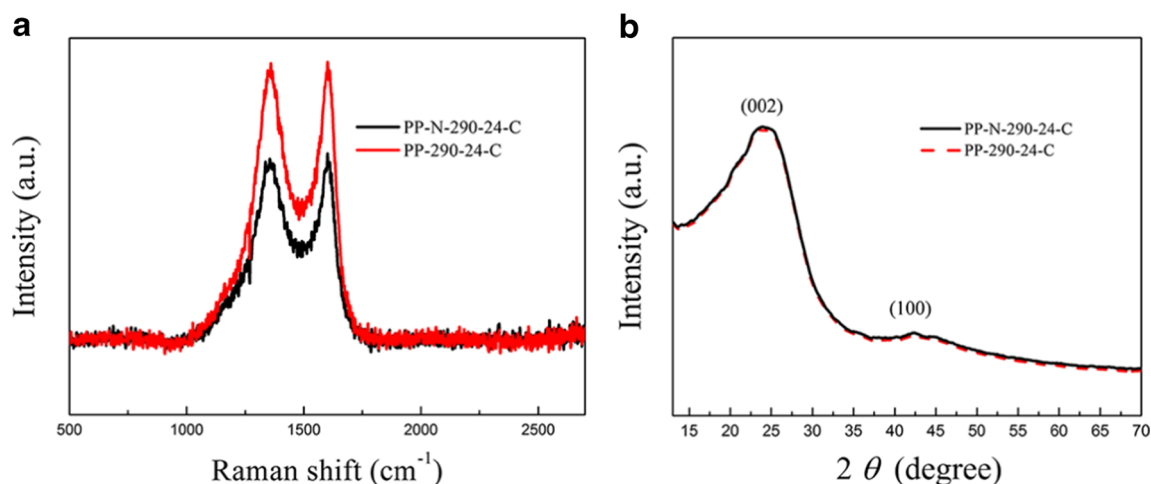


Fig. 7 **a** Raman spectra and **b** XRD pattern of PP-N-290-24-C and PP-290-24-C

Conclusions

In summary, pitch-based anode material has been tested for LIBs after the material characterization and electrochemical optimization, in which stable morphology, rich oxygenic functional groups, and larger interlayer space jointly endow PP-290-24-C electrodes with superb cycling performance. Without doubt, the results reported here are highly dependent on the nature of the starting parent pitch and its existing functionalities. We would expect major differences in oxidative stabilization behaviors from other raw material sources such as coal tar pitch or mesophase pitch. Furthermore, slowing the rate of oxidative stabilization tends to be an effective method in acquiring products of better electrochemical performances, but this rate cannot be extrapolated to infinitely slow as industrial cost is closely related with production time. Therefore, the next major concern of similar research is to explore other cheap and efficient oxidation methods in addition to superior as well as low-cost raw materials we have reported here.

Acknowledgments This research was financially supported by the National Nature Science Foundation of China (51172160, 50902102), the National High Technology Research and Development Program of China (863) (2011AA11A232, 2013AA050905), and the Nature Science Foundation of Tianjin, China (11JCYBJC07500).

References

- Armand M, Tarascon JM (2008) Building better batteries. *Nature* 451:652–657
- Shi W, Lu B (2014) Kirkendall effect synthesis of echinus-like $\text{SnO}_2/\text{SnS}_2$ nanospheres as high performance anode material for lithium ion batteries. *Electrochim Acta* 133:247–253
- Nishijima M, Ootani T, Kamimura Y, Sueki T, Esaki S, Murai S, Fujita K, Tanaka K, Ohira K, Koyama Y, Tanaka I (2014) Accelerated discovery of cathode materials with prolonged cycle life for lithium-ion battery. *Nat Commun* 5
- Zhou G, Li F, Cheng HM (2014) Progress in flexible lithium batteries and future prospects. *Energy Environ Sci* 7:1307–1338
- Zhu J, Zhang G, Gu S, Lu B (2014) SnO_2 nanorods on ZnO nanofibers: a new class of hierarchical nanostructures enabled by electrospinning as anode material for high-performance lithium-ion batteries. *Electrochim Acta* 150:308–313
- Tarascon JM, Armand M (2001) Issues and challenges facing rechargeable lithium batteries. *Nature* 414:359–367
- Dahn JR, Zheng T, Liu Y, Xue JS (1995) Mechanisms for lithium insertion in carbonaceous materials. *Science* 270:590
- Takahashi Y, Oishi J, Miki Y (1994) 35th Battery Symposium in Japan. Extended Abstracts, Paper 2B05, Nagoya
- Sonobe N, Ishikawa M, Iwasaki T (1994) The 35th Battery Symposium in Japan. Extended Abstracts, Paper 2B10, Nagoya
- Fujimoto H, Tokumitsu K, Mabuchi A, Chinnasamy N, Kasuh T (2010) The anode performance of the hard carbon for the lithium ion battery derived from the oxygen-containing aromatic precursors. *J Power Sources* 195:7452–7456
- Stevens DA, Dahn JR (2000) High capacity anode materials for rechargeable sodium-ion batteries. *J Electrochem Soc* 147:1271–1273
- Komaba S, Murata W, Ishikawa T, Yabuuchi N, Ozeki T, Nakayama T, Ogata A, Gotoh K, Fujiwara K (2011) Electrochemical Na insertion and solid electrolyte interphase for hard-carbon electrodes and application to Na-ion batteries. *Adv Func Mater* 21:3859–3867
- Tang K, Fu L, White RJ, Yu L, Titirici MM, Antonietti M, Maier J (2012) Hollow carbon nanospheres with superior rate capability for sodium-based batteries. *Adv Energy Mater* 2:873–877
- Wang H, Wu Z, Meng F, Ma D, Huang X, Wang L, Zhang X (2013) Nitrogen-doped porous carbon nanosheets as low-cost, high-performance anode material for sodium-ion batteries. *ChemSusChem* 6:56–60
- Fu L, Tang K, Song K, van Aken PA (2014) Nitrogen doped porous carbon fibres as anode materials for sodium ion batteries with excellent rate performance. *Nanoscale* 6:1384–1389
- Flandrois S, Simon B (1999) Carbon materials for lithium-ion rechargeable batteries. *Carbon* 37:165–180
- Noel M, Suryanarayanan V (2002) Role of carbon host lattices in Li-ion intercalation/de-intercalation processes. *J Power Sources* 111:193–209
- Xing W, Xue JS, Zheng T, Gibaud A, Dahn JR (1996) Correlation between lithium intercalation capacity and microstructure in hard carbons. *J Electrochem Soc* 143:3482–3491

19. Liu Y, Xue JS, Zheng T, Dahn JR (1996) Mechanism of lithium insertion in hard carbons prepared by pyrolysis of epoxy resins. *Carbon* 34:193–200
20. Zhang LC, Hu Z, Wang L, Teng F, Yu Y, Chen CH (2013) Rice paper-derived 3D-porous carbon films for lithium-ion batteries. *Electrochim Acta* 89:310–316
21. Yang J, Zhou X, Li J, Zou YL, Tang JJ (2012) Study of nano-porous hard carbons as anode materials for lithium ion batteries. *Mater Chem Phys* 135:445–450
22. Li W, Chen M, Wang C (2011) Spherical hard carbon prepared from potato starch using as anode material for Li-ion batteries. *Mater Lett* 65:3368–3370
23. Ni J, Huang Y, Gao L (2013) A high-performance hard carbon for Li-ion batteries and supercapacitors application. *J Power Sources* 223:306–311
24. Park CW, Yoon SH, Lee SI, Oh SM (2000) Li⁺ storage sites in non-graphitizable carbons prepared from methylnaphthalene-derived isotropic pitches. *Carbon* 38:995–1001
25. Piotrowska A, Kierzek K, Rutkowski P, Machnikowski J (2013) Properties and lithium insertion behavior of hard carbons produced by pyrolysis of various polymers at 1000 °C. *J Anal Appl Pyrol* 102:1–6
26. Concheso A, Santamaría R, Granda M, Menéndez R, Jiménez-Mateos JM, Alcántara R, Lavela P, Tirado JL (2005) Influence of oxidative stabilization on the electrochemical behaviour of coal tar pitch derived carbons in lithium batteries. *Electrochim Acta* 50:1225–1232
27. Li Y, Hu YS, Li H, Chen L, Huang X (2016) A superior low-cost amorphous carbon anode made from pitch and lignin for sodium-ion batteries. *J Mater Chem A* 4:96–104
28. Jin J, Yu B, Shi Z, Chong C, Wang C (2014) Lignin-based electrospun carbon nanofibrous webs as free-standing and binder-free electrodes for sodium ion batteries. *J Power Sources* 272:800–807
29. Drbohlav J, Stevenson WTK (1995) The oxidative stabilization and carbonization of a synthetic mesophase pitch, part I: the oxidative stabilization process. *Carbon* 33:693–711
30. Miura K, Nakagawa H, Hashimoto K (1995) Examination of the oxidative stabilization reaction of the pitch-based carbon fiber through continuous measurement of oxygen chemisorption and gas formation rate. *Carbon* 33:275–282
31. Barr JB, Lewis IC (1978) Chemical changes during the mild air oxidation of pitch. *Carbon* 16:439–444
32. Zhao PY, Guo Y, Yu BJ, Zhang Z, Wang CY (2016) Biotechnology humic acids-based electrospun carbon nanofibers as cost-efficient electrodes for lithium-ion batteries. *Electrochim Acta* 203:66–73
33. Biscoe J, Warren BE (1942) An X-ray study of carbon black. *J Appl Phys* 13:364–371
34. Lin Q, Li T, Zheng C, Zhao Y, Song S (2004) Carbonization behavior of coal-tar pitch modified with divinylbenzene and optical texture of resultant semi-cokes. *J Anal Appl Pyrol* 71:817–826
35. Blanco C, Santamaría R, Bermejo J, Menéndez R (2000) A comparative study of air-blown and thermally treated coal-tar pitches. *Carbon* 38:517–523
36. Buiel E, George AE, Dahn JR (1998) On the reduction of lithium insertion capacity in hard-carbon anode materials with increasing heat-treatment temperature. *J Electrochem Soc* 145:2252–2257
37. Silverstein RM, Bassler GC, Merrill TC (1981) In spectrometric identification of organic compounds, 3rd edn. Wiley, New York
38. Mochida I, Shimizu K, Korai Y, Otsuka H, Sakai Y, Fujiyama S (1990) Preparation of mesophase pitch from aromatic hydrocarbons by the aid of HFBF₃. *Carbon* 28:311–319
39. Drbohlav J, Stevenson WTK (1995) The oxidative stabilization and carbonization of a synthetic mesophase pitch, part II: the carbonization process. *Carbon* 33:713–731
40. Stevens DA, Dahn JR (2001) The mechanisms of lithium and sodium insertion in carbon materials. *J Electrochem Soc* 148:A803–A811
41. Ponrouch A, Goñi AR, Palacín MR (2013) High capacity hard carbon anodes for sodium ion batteries in additive free electrolyte. *Electrochem Commun* 27:85–88
42. Jin J, Shi ZQ, Wang CY (2014) Electrochemical performance of electrospun carbon nanofibers as free-standing and binder-free anodes for sodium-ion and lithium-ion batteries. *Electrochim Acta* 141:302–310
43. Zhao J, Zhao L, Chihara K, Okada S, Yamaki J-I, Matsumoto S (2013) Electrochemical and thermal properties of hard carbon-type anode for Na-ion batteries. *J Power Sources* 244:752–757
44. *Lithium batteries: science and technology*, Springer Science & Business Media, 2008
45. Xu K (2004) Nonaqueous liquid electrolytes for lithium-based rechargeable batteries. *Chem Rev* 104:4303–4418
46. Kim C, Yang KS, Kojima M, Yoshida K, Kim YJ, Kim YA, Endo M (2006) Fabrication of electrospinning-derived carbon nanofiber webs for the anode material of lithium-ion secondary batteries. *Adv Func Mater* 16:2393–2397
47. Kim C, Park SH, Cho JI, Lee DY, Park TJ, Lee WJ, Yang KS (2004) Raman spectroscopic evaluation of polyacrylonitrile-based carbon nanofibers prepared by electrospinning. *J Raman Spectrosc* 35:928–933
48. Song LJ, Liu SS, Yu BJ, Wang CY, Li MW (2015) Anode performance of mesocarbon microbeads for sodium-ion batteries. *Carbon* 95:972–977
49. Cao Y, Xiao L, Sushko ML, Wang W, Schwenzer B, Xiao J, Nie Z, Saraf LV, Yang Z, Liu Y (2012) Sodium ion insertion in hollow carbon nanowires for battery applications. *Nano Lett* 12:3783–3787
50. Ding J, Wang H, Li Z, Kohandehghan A, Cui K, Xu Z, Zahiri B, Tan X, Lotfabad EM, Olsen BC, Mitlin D (2013) Carbon nanosheet frameworks derived from peat moss as high performance sodium ion battery anodes. *ACS Nano* 7:11004–11015